ELSEVIER

Journal of Nuclear Materials 241–243 (1997) 52–67

journal of nuclear materials

Hydrogen retention in plasma-facing materials and its consequences on tokamak operation

A.P. Zakharov *, A.E. Gorodetsky, V.Kh. Alimov, S.L. Kanashenko, A.V. Markin

Institute of Physical Chemistry of the Russian Academy of Sciences, Leninsky prospect 31, 117915 Moscow, Russia

Abstract

The current status of research in the area of hydrogen retention and release for the prime candidate plasma-facing materials is briefly reviewed. Physical understanding of the basic problems of hydrogen behavior in the surface layers and material bulk of graphite, beryllium and tungsten is emphasized. The data base in the field obtained in laboratory set-ups permits more thorough consideration of the recent experimental results in large tokamaks. It is known that hydrogen isotopes retention and release has a great influence on tokamak operating conditions and its plasma parameters. The processes occurring in tokamaks with hydrogen participation, such as recycling, fuelling, codeposition, isotopic exchange and conditioning, now can be better understood, explained and controlled. Some consequences of hydrogen isotopes behavior in plasma and plasma-facing materials are described for long pulse tokamak operation.

Keywords: Wall particle retention; Low Z wall material; High Z wall material; Particle fuelling

1. Introduction

Problems of plasma-surface interaction including hydrogen isotope retention and release became of interest since the very first experiments on tokamaks in the Kurchatov Institute [1]. The main attention at pulse duration of 10^{-2}–10^{-1} s in a torus with metal wall was paid to hydrogen chemisorption, chemical reactions at the surface and to the processes of photon-, electron- and ion-induced desorption of hydrogen [2]. The term of hydrogen recycling was introduced for description of the interchange of hydrogen fuel between the plasma and plasma-facing components (PFC) [2,3]. It became important also to take into account the influence of the recycling of such impurities as carbon and oxygen [4].

To get controllable plasma pulses of 0.1–1 s duration, the experimentalists tried to decrease the recycling of hydrogen and impurities and to increase the hydrogen potential capacity of surface layers of plasma-facing materials (PFM). This capacity characterizes the material ability to retain hydrogen during the discharge. At the same time it was desirable to recover the PFM capacity for hydrogen before the next pulse. Therefore the methodology of torus conditioning [5] and thin layer (0.1–0.3 μm) deposition between or during discharges was suggested. For the film deposition, carbon [5,6], boron [7], beryllium [8], lithium [9] and silicon [10] were used. It appeared to be necessary to investigate thoroughly such processes as radiation-induced release of hydrogen [5,11] and sublimation of carbon [12], erosion of graphite and beryllium [13,14], codeposition of hydrogen and carbon [15] and hydrogen and beryllium [16].

When passing on the discharges with duration of 1–10 s and more, at higher temperature of the PFC, it is obvious that retained hydrogen may migrate into the bulk of the material. What amount of hydrogen can be retained in the bulk of the PFM and how much hydrogen can permeate through the PFC into the cooling system of the tokamak? How will the retention and migration processes influence the recycling? These questions stimulate the extensive research of hydrogen behavior in the main chosen PFM: graphite, beryllium and tungsten [17].

In parallel to experimental studies of hydrogen adsorption, solubility and diffusivity in the PFM, the investigation of the PFC material effect on the plasma density

* Corresponding author. Tel.: +7-095 330 2192; fax: +7-095 334 8531; e-mail: zakharov@surface.phyche.msk.su.

PII S0022-3115(96)00494-1

control in tokamaks [18,19] is getting more and more significant.

In the present review the problems of hydrogen behavior in the ion implanted zone and in the bulk are discussed separately for graphite, beryllium and tungsten. The last part is devoted to the analysis of the balance of hydrogen particles and hydrogen fluxes between the plasma and different plasma-facing components of tokamak devices.

2. Hydrogen retention, re-emission and isotopic exchange in the surface layers of plasma-facing materials. Data from experimental modelling in laboratory set-ups

In this part the description of the main results of experiments with ion implantation and their interpretation are presented. These data are important because the hydrogen behavior in the ion implanted zone at saturation level is identical to that in the codeposited layers [15]. Hydrogen behavior in graphite will be reviewed in more detail than that in beryllium and tungsten because the majority of experiments in tokamaks up to now has been performed with graphite components of the vacuum vessel.

2.1. Graphite

Under irradiation of graphite at temperatures T_{irr} = 300–1300 K with hydrogen ions (E = 50 eV to 20 keV, $\Phi = 10^{14}$–10^{15} cm^{-2}) the hydrogen atom is captured by radiation traps with the probability close to unity [20–22]. At fluences $\Phi = 10^{16}$–10^{18} cm^{-2} the hydrogen/carbon ratio reaches a steady-state value of 0.4–0.01 depending on the target temperature (Fig. 1, [23,24]). Such an amount of hydrogen cannot be introduced into graphite from the atomic or molecular gas phase. The real hydrogen profiles at low fluences and simulated ion range profiles in the amorphous carbon coincide satisfactorily [25,26]. When

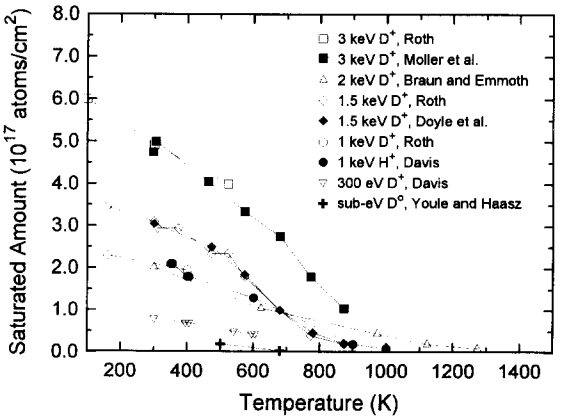

Fig. 1. Saturated amounts of ion-implanted hydrogen isotopes in graphite as a function of implantation temperature [23,24].

the fluence increases the real profiles broaden mainly towards the surface and the rate of reaching the saturated concentration is determined by the ion energy and/or calculated ion range distribution [28]. For ion fluxes of 10^{14}–10^{17} cm^{-2} s^{-1} the upper hydrogen content in the irradiated area remains constant for the given energy and irradiation temperature [21].

As the hydrogen is accumulated in graphite (T = 300–1100 K) the target begins to emit hydrogen molecules and on reaching steady-state the re-emission flux becomes comparable with the incoming ion flux [27]. A characteristic feature of re-emission flux is its relatively slow formation up to steady-state value upon switching on the beam and rapid decrease, up to an order lower, after switching the beam off [28,29]. The desorbing hydrogen flux turned out to be much less than the re-emission flux during irradiation, when the ion beam was switched off. This means that re-emission and retention both are ion-induced processes.

The re-emission of H_2, HD and D_2 molecules created as a result of isotopic exchange has shown that mixing of isotopes being stopped in various parts of the ion projected zone is negligible in surface layers after sequential implantations [30].

Experiments with thermal atomic beams of H [31] for pyrolythic graphite previously saturated with deuterium have convincingly indicated that the composition of the re-emission beam in the process of irradiation underwent considerable changes. At the initial moments, the re-emission was affected only by HD molecules and at the final stages by H_2 molecules. In this connection the conclusion about formation of re-emission molecular flux at the expense of exchange reactions between incoming H particles and deuterium-containing traps at the graphite surface seems to be correct.

These data make it possible to believe that the main contribution to the formation of a re-emission flux is introduced directly by the initial beam. In other words, re-emission is not the consequence of thermal diffusion processes connected with the concentration gradients of moving particles (the beam is switched off). Radiation-induced formation of hydrogen molecules appears to occur near the place where the implanted ion comes to rest. The molecule moves towards the surface of the target through the system of pores or channels and practically without adsorption and dissociation on inner boundaries. The time of movement of molecules towards the surface is much less than the time intervals between subsequent collisions of incoming ions in the molecule migration area.

At temperatures of T = 1300–1500 K the contribution of atomic hydrogen to re-emission becomes dominant [32,33]. At these temperatures the individual H atoms get the possibility to move easily at distances up to 0.1 μm towards the surface and beyond the ion projected range. Can migration atoms give the essential input for bulk retention? The question needs further investigation. It is

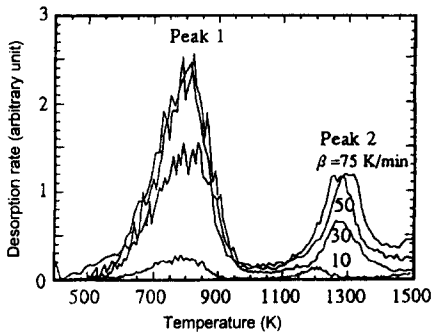

Fig. 2. Thermal desorption spectra of D_2 from high density isotropic graphite exposed to deuterium RF plasma discharge: atom flux 8×10^{17} D/cm^{2}s; fluence 1.6×10^{21} D/cm^2 [36]. Heating rate = 10–75 K/min.

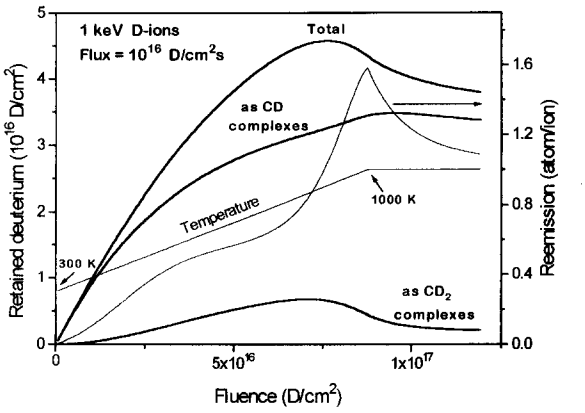

Fig. 3. Calculated content of deuterium trapped in the form of CD and CD_2 complexes (left axis) and deuterium re-emission rate (right axis) at temperatures increase during D-ion bombardment. Heating rate = 70 K/s.

interesting from the scientific point of view but it is not very important for tokamak plasma-facing components if their temperature is less than 1000 K.

Considering the atomic reactions in the stopping zone it is necessary to pay attention to the following experimental results obtained within the range of temperatures of 300–1100 K [42,43]: (1) Existence of two main types of traps containing one or two D atoms (CD and CD_2 complexes); (2) existence of their saturation level under prolonged irradiation; (3) different temperature stability of CD and CD_2 complexes and (4) formation of molecular hydrogen in hydrogen containing traps.

These results were obtained in experiments with different hydrogen loading and heat treatment of graphites by means of thermal desorption spectroscopy (TDS) [34], infra-red spectroscopy (IRS) [35] and depth profiling [26]. One example is given in Fig. 2 [36].

Higher temperature peaks correspond to CD complexes in which deuterium–carbon bond is the sp^2 configuration. CD_2 complexes (lower temperature peak) consist of deuterium atoms bonded with carbon through sp^3 configuration [37]. The data on different thermal stability of CD and CD_2 complexes were used for calculating their steady-state concentrations and re-emission fluxes of molecular hydrogen under increased temperatures of irradiation (Fig. 3). Such calculation [37] and experiments [23] can be useful for the analysis of extended tokamak discharges when the recycling coefficient can exceed unity because of increasing wall tile temperature.

As mentioned above, the formation of hydrogen molecules occurs at localized traps. In the literature for such reaction one uses the term 'abstraction' of hydrogen [38]. The abstraction mechanism of re-emission (at $T <$ 1000 K) is confirmed also by the experiments on isotopic exchange in the implantation zone under sequential D^+ and H^+ irradiation [39], when the HD re-emission rate decreased exponentially with the H content decreasing in the target.

At simultaneous H^+/D^+ bombardment of graphite with different ion energies the extent of HD formation at steady state is quite independent of the separation of the two ion distributions [40], in direct contrast to the conclusions of Ref. [41]. Haasz et al. [33] have proposed a conceptual model which invokes a free atom movement mechanism allowing H/D recombination to take place within the entire implantation zone rather than just at the end of ion range. The model explains successfully the observed complete mixing of H and D during simultaneous H^+/D^+ bombardment at steady state. In our opinion, instead of Haasz expression 'free atom movement' it would be better to use the term 'ion-induced mixing'.

During tokamak operation the outgassing rate of the torus elements between the shots is one of the most important parameters for proper conditioning. In Fig. 4 the relative implanted deuterium amount as a function of annealing time at different temperatures is shown [42].

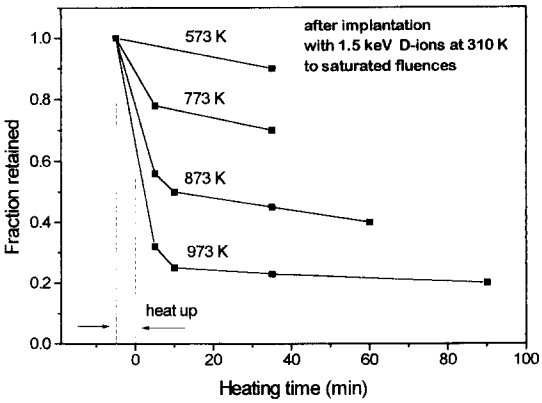

Fig. 4. The relative deuterium amount as a function of temperature and annealing time [42]. For 573 K, data from [43].

The outgassing can be enhanced by helium or carbon ion bombardment of hydrogen containing graphite [43]. At high He ion fluences helium caused only about 25–35% of retained deuterium to be released. Our experiments showed that by means of He-ion irradiation it is possible to remove deuterium only from CD_2 complexes but not from CD ones [44].

Some experimental results obtained allow the assessment of the graphite wall pumping effect for hydrogen particles at an energy of 300 eV and temperatures of 300–500 K. At these conditions the potential capacity of the graphite surface layer is about 3.2×10^{16} atoms/cm^2 or 10^{-3} Torr L/cm^2 = 10 Torr L/m^2. It is known also [21] that the process of hydrogen absorption by graphite is not changed when the particle fluxes increase up to $\sim 10^{17}$ atoms/cm^{2}s. This means that the wall pumping speed is not less than 10–30 Torr L/m^{2}s. The maximal hydrogen release rate under 1 keV He ion treatment with flux 10^{17} He/cm^{2}s is three times less than the wall pumping speed because helium can not remove all implanted hydrogen. The simple isothermal annealing at 600–700 K gives the outgassing rates of 10^{-3} to 10^{-4} Torr L/m^{2}s.

2.2. Beryllium

Similar to hydrogen behavior in carbon materials, in the initial stage of D-ion irradiation at 300 K essentially 100% of ions impinging at the surface of Be sample are retained. Further irradiation results in the re-emission of implanted deuterium. Prolonged implantation leads to the formation of a surface layer saturated with deuterium at the level dependent on the irradiation temperature. Wampler showed [45] that after irradiation at low fluences the release of deuterium under conditions of isochronal annealing occurs in one stage at about 700 K. After irradiation up to saturation one more low temperature stage of the gas release appears around 400 K. Based on the analysis of these data it was deduced that two types of traps for D atoms, with detrapping energies of 1 and 1.8 eV, were created in Be under D-ion irradiation.

Recently, by using transmission electron microscopy (TEM) the near surface microstructure of Be implanted with 3–9 keV D-ions has been studied by Chernikov et al. [46] and Yoshida et al. [47]. It has been found that very fine cavities of ~ 2 nm in diameter are formed in the ion stopping zone during the irradiation at 300 K. Under post-implantation annealing these cavities start to coalesce above ~ 650 K. This result indicates clearly that implanted D atoms interact strongly with radiation vacancies, forming D atoms-vacancies (D-V) clusters stable up to 650 K.

An important point is that the capacity of beryllium matrix to sustain deuterium in the form of D–V clusters is limited by the bubbles development. As has been shown by Alimov et al. [48] for 9 keV D-ion implantation at 300 K the first D_2 bubbles appear when $\sim 1\%$ deuterium

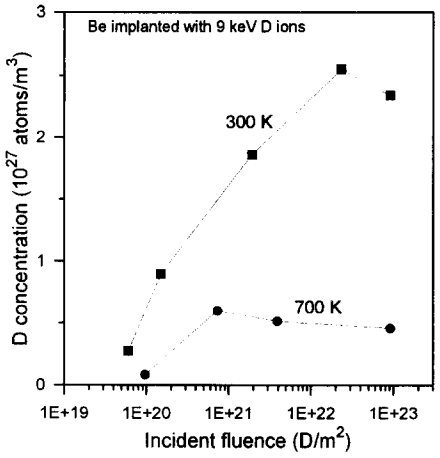

Fig. 5. D atom concentration in the matrix of beryllium at the depth of R_p as a function of 9 keV D-ions fluence for the irradiation temperatures 300 and 700 K.

concentration is attained. Under further irradiation, the deuterium concentration in the matrix at the depth of the ion mean range, R_p, derived from secondary ion mass spectrometry (SIMS) measurements increases gradually and then reaches the saturation level dependent on the irradiation temperature (Fig. 5) while a major part of deuterium implanted is accumulated in the bubbles. It should be noted that limiting values of deuterium concentration in the Be matrix shown in Fig. 5 are overestimated because some part of deuterium trapped in the oxide precipitates makes a contribution to the SIMS signal too.

So the nature of deuterium release from the Be implanted at low fluences seems to be obvious. Subsequent to detrapping from vacancies, D atoms are recaptured by D_2 bubbles from which deuterium has to dissolute before escaping out of the sample. Therefore the dependence of the peak position on the fluence (see peak B in Fig. 6) observed in Refs. [49,50] is understood by a consideration of the microstructure evolution in the course of both irradiation and post-irradiation annealing.

The nature of deuterium trapping at saturated fluences is less understood. Chernikov et al. [46], discussing the data on deuterium re-emission reported in Ref. [51], have speculated that the abrupt re-emission of implanted deuterium from beryllium irradiated with D-ions at 300 K is governed by a partial gas escape from the zone of interlinked gas bubbles when it touches the surface. Thus the near surface layers of the Be sample irradiated at room temperature up to re-emission onset have a large open porosity. In [50] attention was paid to a good agreement between the low temperature part of the release spectra of deuterium from beryllium irradiated with D-ions (peak A in Fig. 6) and TD spectra of hydrogen chemisorbed on (0001) Be single crystal [52]. It is reasonable to relate the low temperature peak A to desorption of D atoms trapped

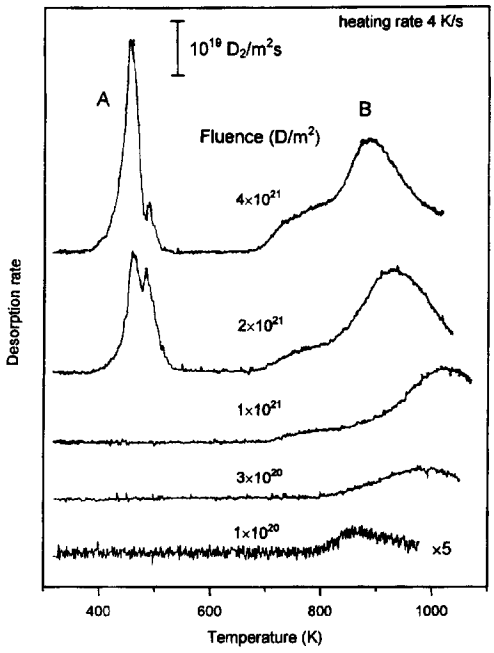

Fig. 6. Thermal desorption spectra of deuterium from TIP-30 Be implanted with 5 keV D-ions up to 4×10^{21} D/m^2 at 300 K. Heating rate = 4 K/s [50].

at the chemisorption sites on the walls of the interlinked D_2 bubbles.

The peak similar to peak A at the same temperature was previously measured on Be samples irradiated with D-ions of energies ranged from 60 to 1000 eV [51]. Authors point out that at an energy less than 100 eV incident deuterons are completely buried in a 5 nm thick oxide layer covering the surface of Be samples etched chemically, while the ion stopping zone for 1 keV D-ions is fully located in the metallic beryllium. This result indicates that the traps, forming both in the original oxide and metal matrix under irradiation up to saturation, appear to be of equal dissociation energy. On the other hand, thermal desorption of deuterium, implanted into thick surface oxide grown by heating of the sample in poor vacuum, did exhibit different behavior: the desorption rate was nearly constant over the whole temperature ramping with no distinct peaks. Microstructural features of the surface oxide layers prepared by various methods may be responsible for different behavior of implanted deuterium.

2.3. Tungsten

Few data have been reported on deuterium inventory in tungsten materials due to D-ion implantation [53–56]. The systematic study of deuterium retention in different types of W samples was done recently by Alimov and Scherzer by means of re-emission (REEM), TDS and nuclear reaction analysis (NRA) measurements [55]. At the beginning of the implantation at temperatures in the range from 300–900 K the re-emission rate first rises rapidly, then increases gradually and reaches the steady-state level only at very high fluences. After termination of D-ion implantation the re-emission curve reduces to several percents and only a fraction of the retained D is released within 10 min after beam switch-off. The amount of deuterium retained in the different W samples after D-ion implantation up to saturated fluences at the different temperatures, as measured by REEM and TDS, is presented in Fig. 7. The retained amounts of deuterium obtained by NRA for the case of 1.5 keV D-ion implantation at 300 K are practically equal for all materials ($\sim 3\times10^{16}$ D/cm^2) which is a factor 2–20 smaller than values determined by the other methods.

It should be noted that at 300 K the amount of retained deuterium in W is of the same order of magnitude as in graphite for the identical implantation parameters (Figs. 1 and 7).

The differences of retained D obtained by REEM/TDS and NRA [55] can be explained both (i) by trapping of implanted D far beyond the implantation zone and (ii) by a slow deuterium release due to diffusion during the interval of 1–2 days between implantation and NRA measurements.

Van Veen et al. [57] reported that 1 keV hydrogen ions implanted into a tungsten single crystal at 350 K are transported to voids located at depth ≥ 10 μm. This indicates a fast diffusive transport of D into traps far beyond the ion range. While in technological W the de-

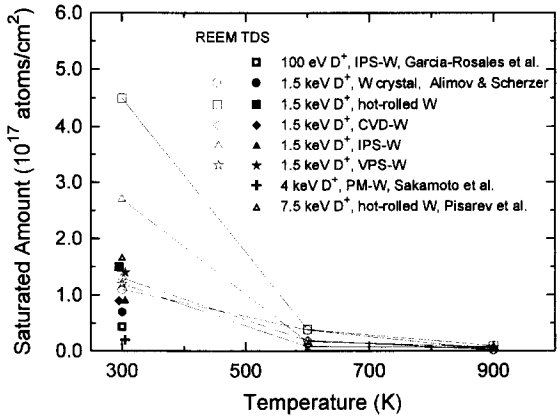

Fig. 7. Saturated amounts of deuterium in different types of W materials implanted with D-ions at energy indicated as a function of implantation temperature as were measured by means of REEM and TDS methods. Data were taken from Refs. [53–56] for W single crystal, hot-rolled W, chemical vapor deposited W coating (CVD-W), inert gas plasma sprayed W coating (IPS-W), vacuum plasma sprayed W coating (VPS-W) and powder metallurgy W (PM-W).

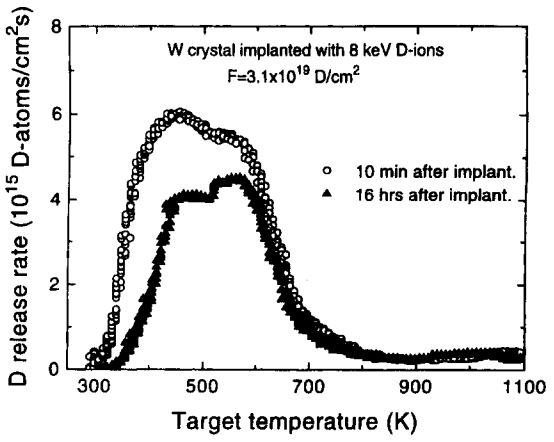

Fig. 8. Time interval dependence of thermal desorption rate of deuterium from W crystal implanted with 8 keV D-ions at 300 K up to saturated fluence [59]. Heating rate = (4.6 ± 0.4) K/s.

fects can be assumed to distribute throughout the bulk of the sample, the concentration of defects in the single crystal is assumed to be very small.

On the other hand, based on experimental results on D re-emission and thermal desorption, García-Rosales et al. [53] proposed a model in which the release of deuterium from W during D-ion bombardment and the thermal release is governed by diffusion. From this model, it also results that a considerable part of deuterium thermally released in the low temperature TDS peak (480–600 K, depending on type of W material) comes from the interstitial sites, while the higher TDS peaks are mainly due to deuterium-vacancy type defects with activation energies of 0.8 and 1.4 eV [53]. Activation energies ranging from 1–1.4 eV for deuterium released from gas filled cavities and vacancies were estimated by Van Veen et al. [57] and Eleveld et al. [58] (note that the activation energy of 1.4 eV corresponds to a release at ~ 700 K in the TDS measurement).

It has been shown in experiment on the influence of time interval between 8 keV D-ion implantation and the TDS measurement [59], that a considerable part (~ 30%) of the total amount of retained D is spontaneously released within 16 h (Fig. 8). A similar result was obtained in TDS measurements 2 and 148 h after switching-off the ion beam for powder metallurgy W implanted at 300 K with 4 keV D-ions [56]. A comparison of the TDS spectra taken after short and long time interval shows that the spontaneously released D belongs to that part which is thermally desorbed between 300 and ~ 450 K and is assumed to be in a solute state. The majority of implanted D, however, is trapped more strongly by defects which already exist initially and/or are created during the implantation.

The retained D measured by NRA is strongly bound to traps which are most probably the defects created during the D-ion implantation in the implanted layer. The larger part of deuterium accumulated in the W samples during the implantation is, however, located far beyond the ion range.

To some extent TDS gives information about the nature of the traps which are responsible for the capture of deuterium in the W samples (Fig. 9). A small fraction (10–30%) of the retained D is mobile. This part is probably still in the solute state (interstitial position) or trapped in low energy trap sites from which it can desorb also at room temperature. In works of Van Veen and Eleveld [57,58], the TDS peaks in the temperature range from 400 to 600 K were attributed to the deuterium release both from deuterium-vacancy complexes and from D_2 filled cavities. We assume that some part of the implanted D is accumulated in ion induced vacancy type defects. Apparently, another part of the implanted D diffuses into the bulk and is captured by lattice imperfections (small cavities, impurity inclusions, etc.). The TDS peak at ~ 950 K observed for plasma sprayed W can be ascribed to the release of chemisorbed atomic deuterium inside the cavities [57].

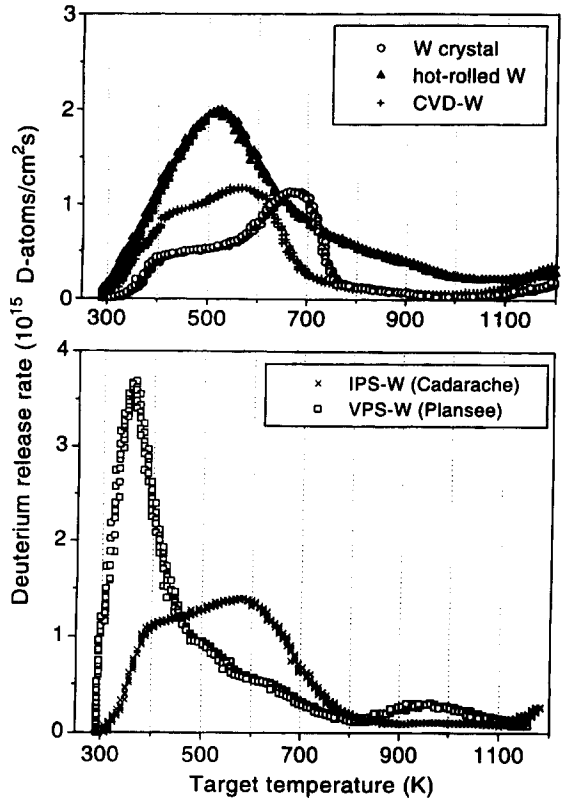

Fig. 9. Thermal desorption rates of deuterium from the W materials implanted with 1.5 keV D-ions at 300 K up to saturated fluences [55]. The TDS curves are given for W single crystal, hot-rolled W, chemical vapor deposited W coating (CVD-W), inert gas plasma sprayed W coating (IPS-W) and vacuum plasma sprayed W coating (VPS-W). Heating rate = (4.6 ± 0.4) K/s.

2.4. Summary

H-ion implantation of graphite to saturation fluence and C/H codeposition as well lead to the formation of C_n–H_m phases stable up to 500–700 K.

H-ion implantation of beryllium leads to the formation of a two-phase system consisting of hydrogen atoms and hydrogen bubbles in the matrix.

The phase formation in near-surface layers in graphite and beryllium provides the hydrogen pumping capacity that leads to the delay in hydrogen re-emission.

Contrary to carbon and beryllium, hydrogen re-emission rate from tungsten starts immediately at the beginning of the H-ion implantation. Saturated hydrogen concentrations in implanted layers are equal to 0.4, 0.3 and 0.25 [102] D/matrix atom for carbon, beryllium and tungsten, respectively, at 300 K and an order of magnitude less at 1000 K. Data for tungsten require additional checking.

3. Hydrogen retention in the bulk of plasma facing materials. Results of experimental modelling

3.1. Graphite

There are only few attempts known to measure the hydrogen content beyond the ion stopping zone. In the case of graphite at $T_{in} < 1000$ K at steady state the hydrogen concentration in the bulk was too low (< 1 appm) for careful analysis of the mechanism of implanted particle migration [60,61]. It is important to notice that the results of modelling experiments with high flux plasma irradiation of graphite need the special discussion. In such experiments it is necessary to take into account the background pressure of molecular hydrogen and to consider 'effective' pressure in the porous bulk [62,68]. The origin of effective pressure is connected with the molecular hydrogen located in the pores of surface layer.

In the simplest model for porous material the outflux transfer through the parallel capillaries with radius r is considered, which is characterized by the parameter of curving. Because of molecular hydrogen appearance in the irradiated area, the 'effective' gas pressure P_{eff} is created and the re-emission flux Γ_{D2} toward the target surface appears. At steady state re-emission Γ_{D2} and irradiation F fluxes are the same. Re-emission flux formation is conditioned by the pressure difference $P_{eff} - P_0$ and the Knudsen coefficient of migration of the molecules through the pores with the average radius r_p: $D_k = (4/3)(2\pi kT/m)^{1/2} \times r_p$. Correlation between the outside pressure P_0 in gaseous phase and pressure P_{eff} inside the stopping zone is given by the expression: $\Gamma_{D2} \times (mkT)^{1/2} = 0.1(P_{eff} - P_0) \times B_p$, where the coefficient B_p is an open porosity of the stopping zone for ions with energy of 100–300 eV. To estimate this value the capillary radius, length and curving are required. In ion implanted condition, the B_p value depends on target temperature and varies between 0.3–0.05 ($T = 300$–1000 K). The product of $\Gamma_{D2} \times (mkT)^{1/2}$ is the outside pressure P_0. This way one could find a correlation between the incoming flux $F = \Gamma_{D2}$, target temperature and characteristic of porosity and effective pressure $P_{eff} = F \times (mkT)^{1/2} \times (10/B_p + 1)$. The effective pressure exceeds the outside pressure near the target over 30–100 times (Fig. 10).

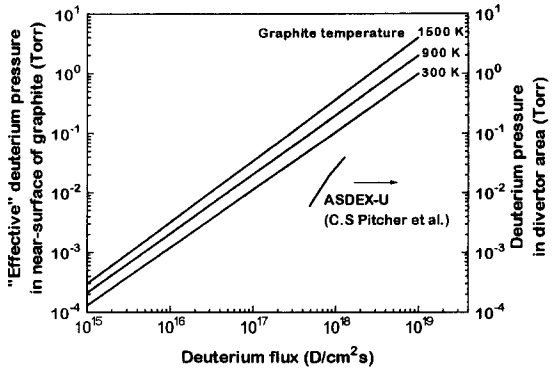

Fig. 10. Calculated steady-state 'effective' deuterium pressure in the stopping zone of graphite and deuterium pressure in divertor area of ASDEX-U [63] as a function of incident deuterium flux. Parameters for calculation: graphite porosity, 0.1; pore radius, 1 nm; stopping zone thickness, 10 nm.

Experiments at divertor conditions in ASDEX-U have shown that there appears to be an approximately linear correlation between the particle fluxes derived from light intensity and the pressure measurements [63]. Experimental points from ASDEX-U are also shown in Fig. 10. The difference can be explained by the reason that the pressure was measured at some distance from the divertor plate.

From the above analysis one could make the following conclusions: (1) The 'effective' hydrogen pressure in the irradiated area P_{eff} and the ion flux F proved to be proportional to each other. For the range of ion flux of 10^{15}–10^{18} D/cm^{2}s the pressure varies between 10^{-4}–10^{-1} Torr. (2) The pressure increases with D-ion energy. For the range of energy of 10–1000 eV and initial flux about 10^{17} D/cm^{2}s the pressure varies in the range of 5×10^{-3}–2×10^{-2} Torr. (3) The pressure is proportional to the square-root of the temperature. (4) In the frames of the ideal gas law the molecular hydrogen concentration in pores in the irradiated area can be estimated as $C = P_{eff}/kT$. Under a pressure of 10^{-2} Torr and a temperature of 1000 K the content should be equal to $(0.5$–$1) \times 10^{14}$ cm^{-3}.

In the hydrogen inventory and permeation problems the stopping zone is considered as source of hydrogen molecules. If the effective pressure is known one can use the data from the literature on hydrogen accumulation kinetics in graphite and also the data on equilibrium hydrogen concentration in graphite [64]. In Ref. [65], the hydrogen inventory was described in a wide range of

temperature as follows. There exists at least three kinds of adsorption sites that are responsible for the hydrogen sorption in graphite.

(i) Carbon interstitial loops with the adsorption enthalpy of -4.4 eV/H_2 (type 1, unrelaxed carbon atoms). These sites are located between graphite layers and are hardly accessible for hydrogen at low temperatures. Transgranular diffusion is necessary for reaching these traps. Causey's experiments [61] showed that at a temperature of 1473 K one hour is necessary to saturate type 1 traps with hydrogen, while this time has been increased up to $\sim$ 20 h for saturation at temperature of 1373 K.

(ii) Carbon network edge atoms with the adsorption enthalpy of -2.3 eV/H_2 (type 2, relaxed carbon atoms). These sites are easily accessible for hydrogen because they are located on the grain boundaries and hydrogen transport is occurred via rapid diffusion through the interconnected pore structure. But saturation of type 2 traps could be limited by adsorption kinetics. Hoinkis' experiments [66,67] showed that tens of hours are necessary for the equilibrium state at a temperature of 1173 K.

(iii) Basal planes adsorption sites with positive enthalpy (type 3 or 'true solution' sites). There is no direct experimental evidence for the existence of hydrogen 'true solubility' in graphites.

Every kind of graphite could be described with its own unique set of traps. From the Causey and Hoinkis experiments it is possible to estimate for nuclear grade graphites the number of Traps 1 as $\sim$ 50 appm [61] and Traps 2 as $\sim$ 200 appm [66]. The number of potential sites for the 'true solubility' (Traps 3) we assume as 5×10^5 appm, or H/C = 0.5, but their filling has very low probability.

This approach proposes that irradiation with neutrons or carbon atoms increases the number of Traps 1 and Traps 2 while the number of Traps 3 remains practically constant. The attempt of estimating the number of Traps 1 and Traps 2 in radiation damaged POCO AXF-5Q graphite based on the experimental data of [65] gives the numbers

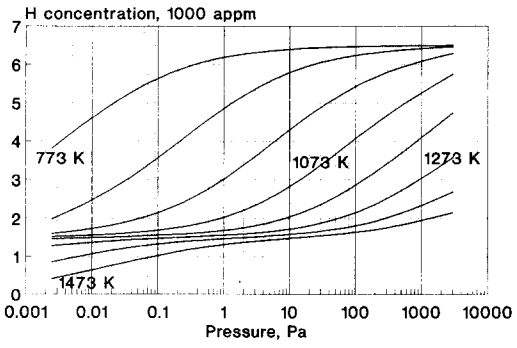

Fig. 11. Calculated sorption isotherm for hydrogen in graphite irradiated with neutrons up to 1 dpa. Calculated 'effective' hydrogen pressure in near-surface layer of graphite: for wall tile 0.1–1 Pa; for divertor tile 3–30 Pa.

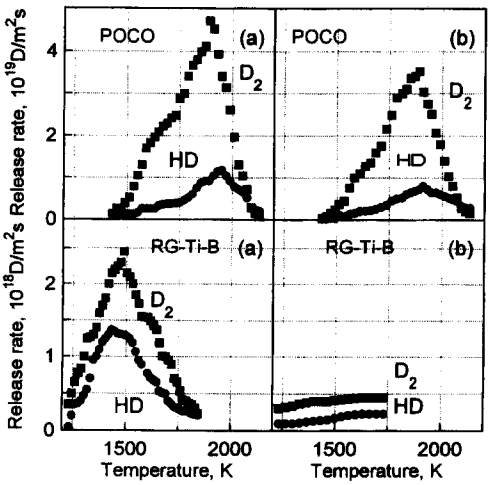

Fig. 12. Thermal desorption of D_2 and HD molecules from POCO AXF-5Q and RG–Ti with 0.1% boron exposed to deuterium plasma (1400 K, ion flux of 6×10^{17} D/cm^{2}s, exposure time of 5 h) before (a) and after (b) mechanical removal of $\sim$ 100 μm thick surface layer [70]. Heating rate = 6 K/s.

of 1.5×10^3 and 5×10^3 appm for Traps 1 and Traps 2, respectively. With that assumption we have calculated the hydrogen inventory for the graphite in a wide range of temperatures and pressures (Fig. 11).

For an estimation of hydrogen retention in porous graphite for ITER conditions a value of the 'effective' pressure inside graphite is needed. In [68] the deuterium bulk retention in POCO exposed to the deuterium plasma (ion flux = 3×10^{17} D/cm^{2}s, 6 h) at 1400 K was studied by TDS. Then these samples were exposed to D_2 at 1400 K for 6 h at deuterium pressure in the range from 0.04–1.3 Pa. The 'effective' pressure corresponds to that D_2 pressure which yields the same bulk deuterium concentration as the plasma exposure and was about 1 Pa. This measurement of hydrogen pressure allows to estimate the equilibrium hydrogen inventory in irradiated graphite yielding values as $(1–3) \times 10^3$ appm. These estimations are very close to the Federici data [69]. Contrary to porous POCO, the bulk deuterium inventory in high density RG-Ti graphite is not detected by TDS (Fig. 12) [70]. It seems likely that deuterium cannot penetrate into the bulk of such graphites.

3.2. Beryllium

There are several computer codes to evaluate tritium inventory in PFCs and tritium behavior in neutron irradiated beryllium as well. Nevertheless, there is a lack of consistent data on hydrogen solubility, diffusion and interaction with defects which gives no grounds for reliable prognosis.

At least two regions in the PFMs are distinguished when dealing with modelling of the tritium inventory

therein [71]. The first one is a near-surface layer modified under plasma impact through redeposition, ion-induced oxidation and ion-induced damage. These layers are formed on the sample surface in laboratory experiments on plasma- [72] and ion-driven [73] deuterium permeation through beryllium and in the current tokamaks as well [74]. The porous layer much thicker than the mean implantation depth for incident ions was developed in a near-surface region of Be samples irradiated with 1 keV D-ions at ~ 700 K [73]. In the authors' opinion these layers may be responsible for the extremely low permeation flux and the prolonged breakthrough time observed. In the above experiments D-ions were assumed to impinge at the clean metal surface. On the other hand, a thick oxide layer (~ 0.9 μm) composed partially of beryllium carbide grew on the surface of the sample exposed to 100 eV D-ion flux from RF plasma at 673 K [72]. In this regard the attempt, made in Ref. [75] to clarify the vacuum-beam conditions when either oxide or metal beryllium appear on the sample surface under prolonged H and Ar ion irradiation, is worthy of notice.

It should be mentioned that hydrogen isotopes behavior in BeO relevant to tokamak operation attracted less attention of the investigators than beryllium. Up to now, there are only two works (made in the same laboratory) concerning the forming of deuterium saturated layers in BeO irradiated with 1–10 keV D-ions [51,76]. Deuterium solubility in the near surface oxide layers of Be samples has been evaluated in [77]. Moreover, it is noted that oxidation of beryllium in atomic or molecular deuterium atmosphere contained oxygen results in the significant deuterium incorporation into oxide [78,101]. So, with the poor database the tritium behavior in BeO is difficult for modelling. Additional experiments, in which the results of permeation measurements are accompanied with the data on tritium inventory in the bulk of the same samples, are desirable and appear to be in preparation at the TPE facility [79].

The second region is the bulk of PFMs, wherein neutron effects must be taken into account as far as ITER issues are considered. Modelling of tritium migration and trapping in this region would be reliable provided the fundamental properties of hydrogen in beryllium have been defined. However, solubility and diffusivity constants measured at the different laboratories are varied widely, being significantly influenced by the sample characteristics [80]. There are evidences for trapping of hydrogen by radiation vacancies (see Section 2.2), oxide inclusions and gas bubbles filled with both hydrogen and helium [49]. Helium generated in beryllium under neutron irradiation at elevated temperatures, just as in other metals, seems to be collected in the bubbles, while at the lower temperatures, exists in the form of HeV clusters. There is reason to think that at 400–700 K (of interest for the first wall PFCs of ITER) helium occupies all available vacancies. How strong tritium, permeating through the PFCs, will be trapped by HeV clusters is not yet understood. Therefore, the energetics of helium-induced trapping of hydrogen in beryllium needs a further consideration.

3.3. Tungsten

For tungsten the data base of solubility, diffusivity, and trapping of hydrogen isotopes is still poor [17]. Due to the high melting temperature, W is produced by different methods (sintering, chemical vapor deposition, plasma spraying, etc.) which introduce many impurities and lattice imperfections. Together with ion induced damage these defects act as trapping sites. Therefore, diffusion and solubility may be influenced by the manufacturing process and the sample history.

The solubility and diffusion constants for hydrogen in tungsten were derived by Frauenfelder [81] from degassing of sintered W which was pre-loaded with hydrogen and by Kizu et al. [82] from permeation experiments. The deuterium diffusion coefficient for 300 K was estimated by García-Rosales et al. [53] from the comparison of re-emission and TDS results for 100 eV D-ion bombardment of hot-rolled W with model calculation.

Experiments described in Section 2.3 (REEM/TDS and spontaneous D release after beam switch-off) indicate that hydrogen penetrates into the bulk at distances of some microns. Diffusion coefficients for 300 K estimated by García-Rosales et al. [53], 9.8×10^{-14} cm^2 s^{-1}, and determined by Kizu et al. [82], 2.9×10^{-15} cm^2 s^{-1}, are several orders smaller than is necessary for a diffusion length > 1 μm during the D-ion implantation time of $\sim 10^4$ s at room temperature. On the other hand, the extrapolation of diffusion data of Frauenfelder [81] gives a diffusivity of 1.1×10^{-9} cm^2 s^{-1} at 300 K which is sufficiently large for the explanation of the results.

3.4. Summary

An 'effective' hydrogen pressure of 10^{-2}–10 Torr appears in the near-surface layers of graphite materials as a result of interaction with the hydrogen plasma. The pressure spreads through the open pores system. This pressure and temperature are responsible for the kinetics of hydrogen sorption and the hydrogen concentration value in the bulk of graphite (or CFC). In the lack of open porosity the bulk hydrogen retention in graphite (like RG–Ti) is rather complicated at $T < 1300$ K.

Hydrogen accumulation in bulk beryllium under plasma exposure is governed by hydrogen concentration in the stopping zone, its diffusivity in the matrix and the concentration of traps of metallurgical and/or radiation origin. The surface development and oxide layer formation can significantly influence the H boundary concentration.

Contrary to beryllium, under plasma exposure the processes of hydrogen retention and transport into the bulk of tungsten are less influenced by surface modification. The hydrogen diffusivity in tungsten is much higher than in beryllium.

Quite reasonable assessments of hydrogen inventories (including permeation) in prime candidate materials are reported recently by Federici et al. [69].

4. Hydrogen retention in plasma-facing components and its influence on fusion device operation

4.1. Hydrogen isotopes retention in tokamak torus

In JET experiments in C- and Be-phases for one discharge, the necessary fuelling was about $(8–10) \times 10^{21}$ atoms per pulse and an average retention of 50–80% of the fuelling gas (i.e., $(5–8) \times 10^{21}$ atoms). About half of the retained gas was released during pauses between shots [83]. If the JET torus surface is about 2×10^6 cm^2, during one discharge the torus surface absorbs about 10^{15} D-atoms/cm^2 or 1–2 monolayers of deuterium. Usually during the campaign from 10^3 up to 2×10^3 shots were made. If the deposition rate is constant, the wall will accumulate after 10^3 discharges up to 10^{18} D-atoms/cm^2. Indeed such areal densities of hydrogen isotopes were found in the surface layers of graphite and beryllium tiles after the machine was opened [74,84].

JET experiments have shown that in view of the higher wall pumping during the discharge and the higher fractional recovery afterwards, Be is a more suitable PFM than graphite as far as deuterium recycling is concerned. An indication that the surface process dominate the outgassing after the discharge ($T \approx 600$ K [83]) came from the observation that the deposition of thin Be coating (10–20 nm [85]) on the C walls of JET is sufficient to permanently change the deuterium retention/release characteristics, as observed from behavior during discharges and the percentage released after pulse.

The recent measurements of hydrogen retention in graphite cladding at JT-60U after operation phases including 2168 D_2 and 1004 H_2 discharge shots [86] are in agreement with data from JET. The retention of deuterium for each tile was distributed between $6 \times (10^{16}–10^{17})$ cm^{-2}. The highest deuterium retention was observed in the tile on the outboard and lower part of the first wall. The D detection for the divertor plate installed in the neutral zone was almost half the value of the D contained in wall tiles. This result suggests that the surface of the divertor plate was heated up to around 1000 K. About 150 hydrogen discharges were performed just before the end of operation. Therefore, inside the divertor and the first wall tiles a relatively large amount of hydrogen is remaining. As the result the ratio of H/D was between 0.45 and 0.65. The revealed correlation between oxygen and deuterium amounts indicates that the codeposition processes of oxygen, deuterium and carbon predominate comparing to ion implantation.

Additional information about the codeposition processes is obtained from the experiments where the average influx and outflux are known. In this connection let us consider the experiments on Tore Supra [87]. In the 1992 campaign, 2333 discharges were performed. The average discharge duration was about 10–15 s. Long term Si and C-samples have been installed on the inner wall. Surface analyses have shown that the high deuterium concentration ($> 10^{18}$ D atoms/cm^2, and $> 10^{24}$ D atoms in total wall inventory) was due to codeposition with carbon atoms (1.8×10^{19} C atoms/cm^2). There are given are the following estimations for codeposition process [87]. At average discharge duration of 10 s and ion flux to the wall of 10^{18} cm^{-2} s^{-1} the integrated flux over 2000 tokamak discharges is about 2×10^{22} cm^{-2}. With carbon concentration in the scrape-off-layer of 5% [88], the carbon deposited is only 1% of the carbon flux, or in other words carbon recycling coefficient is about 0.99 (hydrogen recycling coefficient is higher than 0.9999). Thus the accumulation of hydrogen isotopes in the torus occurs as a result of simultaneous impact of hydrogen and impurity fluxes, including carbon. In average the impurity flux is about 0.05–0.1 of hydrogen isotopes flux.

4.2. Hydrogen isotopes exchange in tokamaks

The tokamak experiments indicate that the hydrogen isotope areal density in PFM usually is 3–10 times higher than the saturated that is obtained in modelling experiments with ion beams at energies of 0.1–300 eV (Fig. 1). The general conclusion is that this difference is caused by parallel hydrogen ion impinging and codeposition of hydrogen and impurities, e.g., carbon, boron or lithium. Probably, the lithium injection in tritium experiments on TFTR is one of the reasons for higher retention of tritium in wall torus [89].

Considering the inventory of hydrogen isotopes in the codeposition process, the question arises, what is the relation between retention rates and isotopic exchange rates?

In modelling experiments with H/D ion implantation into graphite the isotopic exchange terminates completely at the integral fluences of 3–5 fluences of saturation [37]. As a rule in large tokamaks the maximal concentration in the near-surface layer in graphite and beryllium PFC is reached after two to three 10 s discharges (ion energy at edge plasma about 100 eV). It should be noted that the total content of deuterium and the thickness of the saturated layer grows with the increase of number of shots because the simultaneous codeposition process takes place.

Let us consider the preliminary tritium experiment (PTE) performed in JET [83,90,91]. In the initial T/D discharge about 10^{21} T-atoms and 3×10^{22} D-atoms ($\sim$ 500 Torr L) were introduced in the torus. Short term tritium retention after the PTE was 7.5×10^{20} T-atoms. During the subsequent clean-up phase the amount of tritium released per discharge decayed with shot number N roughly as $\exp(-N/N_0)$ with $N_0 = 10$ for the first 10 discharges and $N_0 = 55$ for the next 100 discharges. It

should be noted that dual decay constants have been also observed for H/D changeover experiments in TFTR. About 150 tokamak discharges after the first introduction of tritium in the JET torus, it was sufficient to reduce the in-vessel tritium inventory to a level of 1.8×10^{20} T-atoms.

Probably the initial fast stage of tritium recovery is due directly to ion implantation of deuterium particles from edge plasma in the surface of torus. From another side, the second slow decay of tritium exchange could be connected with the parallel passing process of impurity codeposition. The part of tritium becomes less accessible for isotopic exchange.

This process was simulated using a multireservoir model which splits the accessible hydrogenic particles into two groups, each having a different rate of exchange of particles with plasma [90].

The fast stage of isotopic exchange is displayed most completely in the experiments with sequential H/D fuelling in the JET experiment, when the whole surface of the torus is covered by hydrogen. In the JET T/D exchange experiment tritium occupies about 1% of all potential traps (10^{23} traps/torus of area 200 m^2). So, in the T/D experiment the second phase of the exchange is expressed more evidently due to codeposition.

It is necessary to note that the slow stage of the D/H exchange was analyzed recently in JT-60U [92]. A series of 400 H plasma discharges has reduced the deuterium influx to 0.03 of that in the initial phase.

In general, the isotopic exchange experiments in tokamaks point out the essential role of codeposition processes in plasma-surface interaction.

4.3. Fuelling and recycling

In modern tokamaks the average time, during which plasma particles are confined is in the range from 10^{-3} to 0.3 s and always short compared to the discharge times. Thus, on average, fuel particles must be replaced many times (up to 30–100 times) during a discharge and the mechanism of refuelling is important. Edge refuelling which is carried out by gas puffing tends to result in rather flat plasma radial profiles. On the other hand, achievement of fusion condition in the core plasma can be facilitated by the creation of peaked plasma concentration (n) and temperature (T) profiles (for example, in the supershot regime [93]). This can be achieved by core refuelling using fast pellets of frozen hydrogen or by neutral beam injection (NBI).

If external neutral sources, such as a gas inlet, are turned off and particles come to the plasma from the torus wall or limiter, the constancy of plasma density is considered to be maintained by recycling. In other words, hydrogen isotope exchange between plasma and internal surfaces of torus is called 'hydrogen recycling'. The recycling coefficient R is the ratio of returning hydrogen flux to the incident flux. $R < 1$ means that less hydrogen returns to the plasma from the wall than reaches it. This regime is called wall pumping. In this case the steady state of plasma can be reached by external core or edge refuelling. If $R = 1$ the steady state of plasma can be maintained when the external fuel source is switched off. If $R > 1$, for permanent in time n and T across the torus it is necessary to use the external pumping to remove a part of fuel particles from torus [94].

In modern tokamaks (JET, Tore Supra, JT-60, TFTR, DIII-D and some others) the pulse duration in routine regime is about 1–10 s. To maintain the constant value of plasma concentration and temperature at wall pumping the rate of hydrogen flux introduced from the external sources is about 10–300 Torr L/s (1 Torr L $= 3.2 \times 10^{19}$ molecules). For long shot, 62 s, at Tore Supra, more than 600 Torr L are necessary to maintain the plasma density, with a gas influx of about 10 Torr L/s. Operating ITER at 1500 MW of fusion power produces about 15 Torr L/s of helium ash (the global ^{4}He particle confinement time 28 s [95]), which requires a fuel particle removal rate of about 30 Torr L/s.

It is interesting to note that for such tokamaks as TFTR, Tore Supra and DIII-D, in steady state regime during the discharge there are 3–15 Torr · L of hydrogen molecules in the plasma and about 10^3 Torr · L of hydrogen isotopes in the torus wall. The ITER inventory in plasma is estimated to be about 3×10^3 Torr L of D/T particles [95] while the wall can retain 2×10^6 Torr L D,T/ton Be $\times$ 1% swelling.

4.4. Exchange fluxes between plasma and plasma-facing components

4.4.1. Exchange fluxes in L-mode

One of the main questions of plasma-surface interaction is: how the hydrogen retained in the PFM surface layers can influence the pulse formation?

It is nearly a universal observation in tokamaks with carbon limiters that the application of power, whether in form of ohmic, ICRF or NB heating, results in increased influxes of deuterium and carbon from the limiter and a subsequent increase in the plasma density. The particles exchange between plasma and limiter in L-mode was studied in detail in TFTR experiments with the heating of ohmic plasma by means of NBI [96]. In TFTR the plasma was in contact mainly with graphite limiter of total area about 22 m^2. The main results are shown in Figs. 13 and 14. After deuterium NBI (flux 20 Torr L/s) with 8 MW power for 0.3 s the plasma steady state was reached when the outflux and influx were equal to each other. The electron concentration remains constant during 1 s. At the same time it was observed that the influxes of deuterium ($\sim 8 \times 10^{21}$ D-atoms/s) and carbon ($\sim 3 \times 10^{21}$ C-atoms/s) particles were sufficiently higher than the initial flux of injected neutrals ($\sim 6 \times 10^{20}$ D-atoms/s). The subsequent numerical treatment of the plasma measurement results showed that the D amount in the plasma

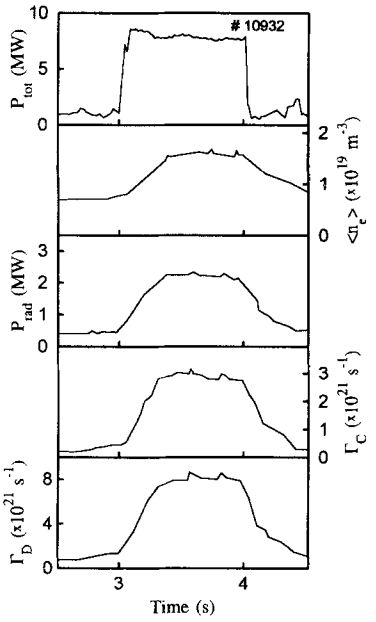

Fig. 13. The time evolution of discharge 40932 (TFTR) during ~ 8 MW of neutral beam injection: $R_0 = 2.60$ m, $a = 0.95$ m, plasma current $I_p = 1.4$ MA, toroidal magnetic field $B_T = 4$ T [96].

$(6 \times 10^{20}$ D-atoms) was much less (~ 30 times) than the D particles amount in the graphite 'reservoir' ($\sim 2 \times 10^{22}$ and D-atoms).

With injection power increasing up to 20 MW (Fig. 14) the recycling fluxes from the limiter increased proportionally, meanwhile Z_{eff} of the discharge and the edge plasma temperature being constant. At these conditions the significant part of injected power was spent for radiation and heating of carbon ions. Thus, the discharge is to a large degree dominated by edge effects, i.e., recycling of fuel and the production of carbon impurities at the limiter surface. These phenomena are undesirable as the potential fusion yield of the discharge is reduced.

4.4.2. Exchange fluxes in supershot plasmas

Is it possible to avoid the edge effects in plasma which are typical for the L-mode discharge? How do we attain the conditions for recycling control? In the last series of experiments in TFTR the scientists tried to decrease the edge recycling by preliminary removal of hydrogen isotopes from the limiter, for example by helium conditioning [97,98] at which the deuterium release from the graphite wall is caused by sputtering. Moreover it was desirable to diminish the carbon and oxygen influxes into the central plasma (in L-mode the ratio of carbon flux to deuterium flux was about 0.25–0.3). To decrease the recycling and to suppress the carbon erosion, lithium pellet injection during ohmic discharge was suggested (3×10^{20} Li-atoms/pellet). During one pellet injection the lithium monolayer was formed on the torus walls.

Li pellets injected at 1 s before NBI into supershot plasmas lead to substantial enhancements in the neutron rate, plasma stored energy, ion temperature and energy confinement time during NBI. Reductions in the edge density resulting from lithium pellet wall conditioning lead to improved NB penetration, which then peaks up the density profile and improves confinement. Sputtering yield calculations indicate that a layer of Li on C significantly reduced the carbon sputtering yield [97].

Analysis of deuterium particle fluxes balance was performed for the discharge of 1 s duration with NBI heating power 25 MW [99]. The first wall was well conditioned and Li-pellet was injected before the NBI. At stationary stage of the discharge the number of D-ions in plasma was about 5×10^{20}. Meanwhile the influx from limiter into SOL was about 10^{22} s^{-1}, the wall recycling coefficient being 0.85 [99]. In our point of view the deuterium influxes in L-mode and in the supershot regime differ insignificantly. However in the supershot regime the limiter is a limited source of deuterium, differing from L-mode when the deuterium amount in the limiter is higher than in the supershot regime. Apparently the main role for improvement of discharge parameters can be attributed to reducing of graphite erosion (up to three times) as a result of lithium adsorption [97].

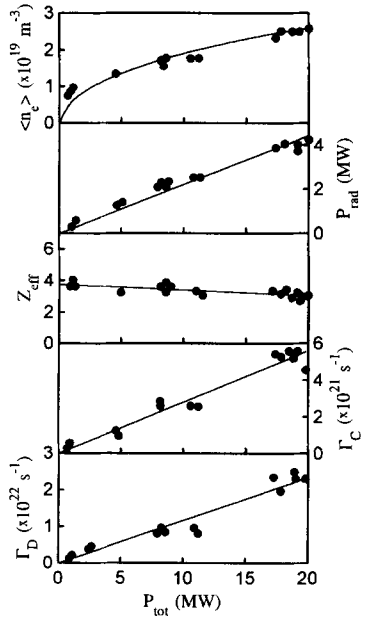

Fig. 14. The scaling of plasma density $\langle n_e \rangle$, radiated power P_{rad}, Z_{eff}, carbon Γ_C and deuterium Γ_D influxes from the limiter with total input power P_{tot}: discharges 40927–40945 (TFTR), $R_0 = 2.60$ m, $a = 0.95$ m, plasma current $I_p = 1.4$ MA, toroidal magnetic field $B_T = 4$ T [96].

The successful experiments in TFTR in the supershot regime allowed to carry out the well-known experiment with tritium injection and to obtain 6 MW neutron power in one shot [89]. A very low total recycling (< 0.75) for all hydrogen isotopes was typical for tritium discharges. At the same time due to initial tritium absence in the machine the tritium recycling was less than 0.05 in the series of 10 shots. In average for the whole campaign (65 shots, 3.5×10^{22} T-atoms) the steady state has not been achieved for tritium between the core plasma and limiter. In analogous preliminary experiments with deuterium discharges 100% recycling was observed. This discrepancy may be explained by large total energy (including higher ion energy) produced in tritium discharges and by increase of codeposition input to tritium retention in torus. The tritium experiments in TFTR have shown that the limiter conditioning by depleting the limiter surface of hydrogen isotopes and Li pellet injection to reduce the carbon influx are critical to the attainment of supershots and high fusion power. The low tritium recycling from the limiter reduces core plasma reactivity; tritium rich NB injection is required to obtain the optimum 50:50 DT density ratio [89].

4.5. Particle exhaust with external pumping

We have already noted during supershot analysis in TFTR that the wall pumping is ultimately a transient effect and by itself not suitable for steady state particle exhaust. Therefore, external exhaust techniques with pumped divertors and limiters are being developed in tokamaks DIII-D and Tore Supra [94,100]. Tore Supra is a graphite machine in which the wall particle inventory usually dominates the plasma inventory by more than an order of magnitude. As an example let us consider the experiment in Tore Supra when the detailed analysis was made for the particle fluxes between the separate components of the machine (ohmic discharge with 1.5 MA plasma current, 4 T toroidal field, deuterium prefill and gas puff, and a wall temperature of ~ 420 K).

The particle balance for discharge 10450 (Fig. 15) was evaluated by dividing the shot into three parts. During phase (1) the exhaust was minimal due to the low pressure and most of the gas was absorbed by the wall. In phase (2) the difference in the fuelling rate between without and with pumping discharges was balanced by the external exhaust. During phase (3) the gas puff had been turned off and the exhaust rate greatly exceeded the decay rate of plasma. The only plausible source for this extra gas, which was removed in addition to the gas from density decay, was the wall inventory. It has been known that graphite wall can provide strong fuelling to the plasma. The result of Tore Supra indicated that, combined with external exhaust techniques, the wall could also directly supply particles to the exhaust gas. From a different perspective the external particle exhaust not only controls the particle content of the plasma, but also controls the wall inventory.

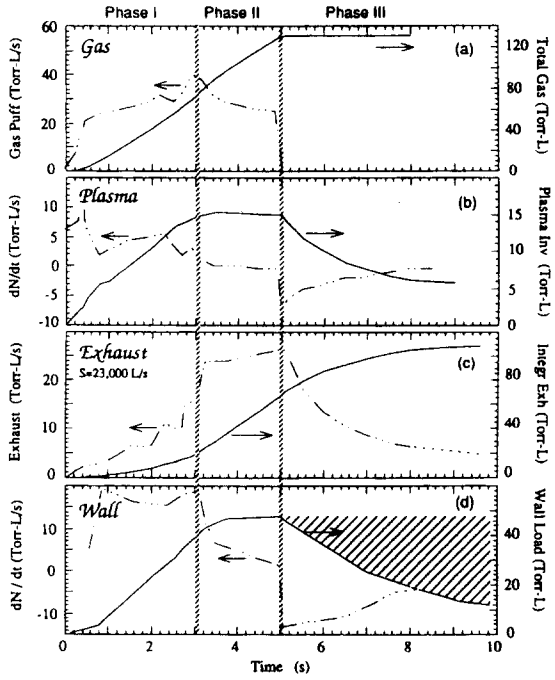

Fig. 15. Particle balance with pump limiter exhaust and gas puffing for shot 10450 (Tore Supra): (a) gas puff, (b) density evolution, (c) pump limiter exhaust and (d) inferred wall load [99].

This effect indicates possibilities for continuous simultaneous wall conditioning during a discharge with external exhaust.

An analogous result has been obtained in DIII-D with pumped divertor. During the pumping discharges the wall could return about 50–80 Torr L of gas.

4.6. Summary

To conduct a single 10 s discharge in a contemporary large tokamak as a rule about 100 Torr L fuel molecules are introduced into the torus. Approximately 50–80% of input gas is immediately captured by the wall. For the pause between the shots, about 1000 s, when gas release takes place, for each discharge the retained hydrogen amount is about 30 Torr L (or $\sim 2 \times 10^{21}$ particles), i.e., 1/3 of input gas particles. At a total wall area of 10^6 cm^2 such quantity of retained particles corresponds to one to two monolayer coverage of the torus by sorbed hydrogen. During the campaign of sequential discharges, the amount of retained gas increases continuously with a rate 1–2 H monolayer per shot without noticeable saturation tendency in a series of 10^3 discharges. At the same time practically all hydrogen retained participates in the processes of isotopic exchange.

During the discharge it is necessary to minimize the hydrogen and impurity recycling and to provide the maximal wall pumping capacity. In the intervals between dis-

charges it is desirable that PFCs would reject back almost all retained hydrogen. The search of optimal dynamic equilibrium regime results in elaboration of a number of techniques which enable to enhance the hydrogen release from PFC surface layers and to increase the wall pumping capacity. These are helium/oxygen conditioning, RF conditioning, particle control with external pumping of limiter/divertor, Li-pellet injection, Be evaporation.

5. Conclusions

(1) For single discharge with duration of 1–10 s in large contemporary tokamaks $(1–3)\times 10^2$ Torr L of hydrogen it is necessary to supply into torus. Under steady state regime plasma contains 10–15 Torr L, but wall contains 40–100 Torr L of hydrogen. In this regime the rates of particles exchange between plasma and wall can reach 100 Torr L/s.

(2) Relaxation times of hydrogen fluxes in respect to absorption (wall pumping) or desorption (wall fuelling) proves less than 0.1 s. During the period mentioned, the wall could transfer from the fuelling state ($\sim$ 30 Torr L/s) into the pumping state ($\sim$ 60 Torr L/s) under instant injection of a hydrogen pellet, helium or NB. Quantitative comparison of the data of wall fuelling rate with the laboratory results on radiation-induced desorption is essential for operation of future larger devices.

(3) During long pulse discharges (scale of 100 s) the wall or limiter accumulates hydrogen up to 100 Torr L per single discharge, but no wall saturation is observed (e.g., in Tore Supra). In these conditions uncontrollable recycling occurs. The temperature growth in codeposited layers could be one of the reasons of uncontrollable recycling. It is clear that for 100 s discharge active control of the particle flux between plasma and wall as well as active cooling of PFCs are necessary.

(4) Analysis of particle balance processes during the discharge indicates that the PFM surface layers (thickness 10–100 nm) play a very active role. In this connection an important trend is successfully developing, modification of these layers during the shot by light elements passing from carbon to boron, silicon and lithium. In this sense recent experiments on tokamaks and laboratory set-ups show that thin layer composition Li–C is very promising.

(5) During long pulse discharges the presence of codeposited films can change globally the kinetics of retention/release and permeation. Additional modelling experiments devoted to analysis of hydrogen retention in the entire bulk of PFMs under erosion and codeposition conditions are required.

(6) Bulk hydrogen content for all mentioned high density materials is negligible ($<$ 10 appm) compared to that in the surface layers (10^{18} cm^2) without neutron irradiation. When radiation damage appears the hydrogen bulk concentration can increase by 2–3 orders of magnitude.

References

[1] W. Poschenrieder et al., J. Nucl. Mater. 220–222 (1995) 36.
[2] K.L. Wilson, J. Nucl. Mater. 103&104 (1981) 453.
[3] J. Ehrenberg, P. Coad and L. De Kock, J. Nucl. Mater. 162–164 (1989) 63.
[4] P.C. Stangeby and G.M. McCracken, Nucl. Fusion 30 (1990) 1225.
[5] F. Waelbroeck, Vacuum 39 (1989) 821.
[6] J. Winter, J. Nucl. Mater. 145–147 (1987) 131.
[7] J. Winter et al., J. Nucl. Mater. 162–164 (1989) 713.
[8] J. Winter, J. Nucl. Mater. 176&177 (1990) 14.
[9] J.A. Snipes, E.S. Marmar and J.L. Terry, J. Nucl. Mater. 196–198 (1992) 686.
[10] U. Samm, P. Bogen, G. Esser et al., J. Nucl. Mater. 220–222 (1994) 25.
[11] K.L. Wilson and W.L. Hsu, J. Nucl. Mater. 145–147 (1987) 121.
[12] V. Philipps, A. Pospieszczuk and B. Schweer, J. Nucl. Mater. 220–222 (1995) 467.
[13] J. Roth, J. Nucl. Mater. 176&177 (1990) 132.
[14] I. Roth, E. Vietzke and A.A. Haasz, Suppl. Nucl. Fusion 1 (1991) 63.
[15] W. Möller, J. Nucl. Mater. 162–164 (1989) 151.
[16] M. Mayer, R. Behrisch, H. Plank et al., J. Nucl. Mater. (1996) in press.
[17] K.L. Wilson, R. Bastasz, R.A. Gausey, B.K. Brice, B.L. Doyle, W.R. Wampler, W. Möller, B.M.U. Scherzer and T. Tanabe, Suppl. Nucl. Fusion 1 (1991) 31.
[18] J. Ehrenberg, P. Andrew, L. Horbon et al., J. Nucl. Mater. 196–198 (1992) 992.
[19] C. Grisolia, L.D. Horton and Y.K. Ehrenberg, J. Nucl. Mater. 220–222 (1995) 516.
[20] M. Braun and B. Emmoth, J. Nucl. Mater. 128&129 (1984) 657.
[21] J.W. Davis, A.A. Haasz and D.S. Walsh, J. Nucl. Mater. 176&177 (1990) 992.
[22] W. Möller and I. Roth, in: Physics of Plasma-Wall Interaction in Controlled Fusion, eds. B.E. Post and R. Behrisch (Plenum, New York, 1986) p. 439.
[23] J.W. Davis and A.A. Haasz, J. Nucl. Mater. 217 (1994) 206.
[24] I.R. Youle and A.A. Haasz, J. Nucl. Mater. 182 (1991) 107.
[25] K. Morita and Y. Hasebe, Memoirs of the School of Engineering, Nagoya University, Vol. 45 (1993) p. 57.
[26] V.Kh. Alimov, A.E. Gorodetsky and A.P. Zakharov, J. Nucl. Mater. 198 (1991) 27.
[27] B.M.U. Scherzer and V.Kh. Alimov, J. Nucl. Mater. 196–198 (1992) 703.
[28] B.M.U. Scherzer, J. Wang and W. Moller, J. Nucl. Mater. 176&177 (1990) 208.
[29] R. Yamada and Saido, J. Nucl. Mater. 162–164 (1989) 1040.
[30] W. Möller, P. Börgeson and B.M.U. Scherzer, Nucl. Instrum. Methods B19&20 (1987) 826.
[31] E. Vietzke, V. Phillips and K. Flaskamp, J. Nucl. Mater. 162–164 (1989) 898.
[32] P. Franzen, E. Vietzke, A.A. Haasz et al., J. Nucl. Mater. 196–198 (1992) 967.
[33] A.A. Haasz, P. Franzen, J.W. Davis et al. J. Appl. Phys. 77 (1995) 66.

[34] V. Phillips, E. Vietzke and M. Erdweg, J. Nucl. Mater. 145–147 (1987) 292.
[35] P. Koidle, Ch. Wild, B. Dischev et al., Mater. Sci. Forum 52&53 (1989) 41.
[36] Y. Yaita, S. O'hira and K.O. Kuno, Fusion Technol. 28 (1995) 1294.
[37] M.A. Lomidze, A.E. Gorodetsky, S.L. Kanashenko et al., J. Nucl. Mater. 208 (1994) 313.
[38] J.E. Butler, B.D. Thoms and M. McGonigal et al., in: Wide Band Gap Electronic Materials, eds. M.A. Prelas et al. (Kluwer Academic, Netherlands, 1995) p. 105.
[39] S.K. Erents, Nucl. Instrum. Methods 170 (1980) 455.
[40] S. Chiu and A.A. Haaz, J. Nucl. Mater. 196–198 (1992) 972.
[41] W. Möller and B.M.U. Scherzer, Appl. Phys. Lett. 50 (1987) 1870.
[42] Sagara, H. Suzuki and N. Ohyabu et al., J. Nucl. Mater. 220–222 (1995) 627.
[43] W.R. Wampler and B.L. Doyle, J. Nucl. Mater. 162–164 (1989) 1025.
[44] M.A. Lomidze, S.L. Kanashenko, A.E. Gorodetsky et al., J. Nucl. Mater. 212–215 (1984) 1483.
[45] W.R. Wampler, J. Nucl. Mater. 122&123 (1984) 1598.
[46] V.N. Chernikov, V.Kh. Alimov, A.V. Markin et al., J. Nucl. Mater. 228 (1996) 47.
[47] N. Yoshida, S. Mizusawa, R. Sakamoto, and T. Muroga, in: Proc. 7th Int. Conf. on Fusion Reactor Materials, Sept. 1995, Obninsk, Russia, J. Nucl. Mater. 233–237 (1996) 874.
[48] V.Kh. Alimov, V.N. Chernikov and A.P. Zakharov, these Proceedings, p. 1047.
[49] W.R. Wampler, J. Nucl. Mater. 196–198 (1992) 981.
[50] A.V. Markin, V.N. Chernikov and S.Yu. Rybakov et al., in: Proc. 2nd IEA Int. Workshop on Beryllium Technology for Fusion, 6–8 Sept., Jackson Lodge, Wyoming (Lockheed Martin Idaho Technologies, Idaho Falls, 1995) p. 332.
[51] W. Möller, B.M.U. Scherzer and J. Bohdansky, IPP-JET Report No. 26 (1986).
[52] V. Lossev and J. Küppers, J. Nucl. Mater. 196–198 (1992) 953.
[53] C. García-Rosales, P. Franzen, H. Plank, J. Roth and E. Gauthier, in: Proc. 7th Int. Conf. on Fusion Reactor Materials, Obninsk, Russia, Sept. 1995, J. Nucl. Mater. 233–237 (1996) 803.
[54] A.A. Pisarev, A.V. Varava and S.K. Zhdanov, J. Nucl. Mater. 220–222 (1995) 926.
[55] V.Kh. Alimov and B.M.U. Scherzer, J. Nucl. Mater. 240 (1996–1997) 75.
[56] R. Sakamoto, T. Mugora and N. Yoshida, in: Proc. 7th Int. Conf. on Fusion Reactor Materials, Obninsk, Russia, Sept. 1995, J. Nucl. Mater. 233–237 (1996) 776.
[57] A. van Veen, H.A. Filius and J. De Vries et al., J. Nucl. Mater. 155–157 (1988) 1113.
[58] H. Eleveld and A. van Veen, J. Nucl. Mater. 191–194 (1992) 433.
[59] V.Kh. Alimov, B.M.U. Scherzer and P. Franzen, private communication.
[60] A.A. Haasz and J.W. Davis, J. Nucl. Mater. 209 (1994) 155.
[61] R.A. Causey, J. Nucl. Mater. 162–164 (1989) 151.
[62] A.E. Gorodetsky and S.L. Kanashenko, Rep. Inst. Phys. Chem. RAN, Moscow, to NIIEFA, St-Petersbourg, 1991.
[63] C.S. Pitcher, H.-S. Bosch and K. Büchl et al., J. Nucl. Mater. 220–222 (1995) 213.
[64] T. Tanabe and H. Atsumi, J. Nucl. Mater. 209 (1994) 109.
[65] S.L. Kanashenko, A.E. Gorodetsky, V.N. Chernikov, A.V. Markin, A.P. Zakharov, B.L. Doyle and W.R. Wampler, in: Proc. 7th Int. Conf. on Fusion Reactor Materials, Obninsk, Sept. 1995, J. Nucl. Mater. 233–237 (1996) 1207.
[66] E. Hoinkis, J. Nucl. Mater. 182 (1991) 93.
[67] E. Hoinkis, J. Nucl. Mater 183 (1991) 9.
[68] I.I. Arkhipov et al., in: Proc. 7th Int. Conf. on Fusion Reactor Materials, Sept. 1995, Obninsk, Russia, J. Nucl. Mater. 233-237 (1996) 1202.
[69] G. Federici and D.F. Holland, ITER Internal Report Parameter Study for Tritium Inventory and Permeation in ITER Plasma-facing Components, 18 Jan. (1996).
[70] I.I. Arkhipov, B.I. Khripunov et al., in preparation.
[71] G.R. Longhurst, R.A. Anderl, T.J. Dolan et al., Fusion Technol. 28 (1995) 1217.
[72] R.A. Causey, W.L. Hsu, B.E. Mills et al., J. Nucl. Mater. 176&177 (1992) 654.
[73] R.A. Anderl, M.R. Hankins, G.R. Longhurst et al., J. Nucl. Mater. 196–198 (1992) 986.
[74] R. Behrisch, A.P. Martinelli and S. Grigull et al., J. Nucl. Mater. 220–222 (1995) 590.
[75] R. Bastasz, Thin Solid Films 121 (1984) 127.
[76] R. Behrisch, R.S. Blewer, J. Borders et al., Radiat. Eff. 48 (1980) 221.
[77] R.G. Macaulay-Newcombe and D.A. Thompson, J. Nucl. Mater. 212–215 (1994) 942.
[78] V.M. Sharapov, L.E. Gavrilov, V.S. Kulikauskas and A.V. Markin, in: Proc. 7th Int. Conf. on Fusion Reactor Materials, Sept. 1995, Obninsk, Russia, J. Nucl. Mater. 233-237 (1996) 870.
[79] R. Causey, D. Buchenauer, D. Taylor et al., Fusion Technol. 28 (1995) 1144.
[80] A.A. Pisarev, Fusion Technol. 28 (1995) 1262.
[81] R. Frauenfelder, J. Vac. Sci. Technol. 6 (1969) 388.
[82] K. Kizu, T. Tanabe and K. Miyazaki, presented at 7th Int. Conf. on Fusion Reactor Materials, Obninsk, Russia, Sept. 1995.
[83] R. Sartori, G. Saibene, D.H.J. Goodall et al., J. Nucl. Mater. 176&177 (1990) 624.
[84] J.P. Coad, R. Behrisch and H. Bergsaker, J. Nucl. Mater. 162–164 (1989) 533.
[85] G. Saibene, A. Rossi, R.D. Monk et al., J. Nucl. Mater. 220–222 (1995) 617.
[86] S. Amemiya, T. Masuda, T. Ando et al., J. Nucl. Mater. 220–222 (1995) 443.
[87] E. Gauthier, A. Grosman and J. Valter, J. Nucl. Mater. 220–222 (1995) 506.
[88] T. Loarer et al., J. Nucl. Mater. 196–198 (1992) 1078.
[89] D.K. Owens et al., J. Nucl. Mater. 220–222 (1995) 62.
[90] L.D. Horton, P. Andrew, G. Bracco et al., J. Nucl. Mater. 196–198 (1992) 139.
[91] P. Andrew, C.J. Caldwell-Nichols, J.P. Coad et al., J. Nucl. Mater. 196–198 (1992) 143.
[92] M. Nemoto, M. Shimada, N. Miya et al., J. Nucl. Mater. 220–222 (1995) 385.

[93] J.D. Strachan, M. Bell, A. Janos et al., J. Nucl. Mater. 196–198 (1992) 28.
[94] M.A. Mahdavi et al., J. Nucl. Mater. 220–222 (1995) 13.
[95] R. Behrisch, Suppl. Nucl. Fusion 1 (1991) 7.
[96] C.S. Pitcher, R.V. Budny, K.W. Hill et al., J. Nucl. Mater. 176&177 (1990) 285.
[97] J.A. Snipes, E.S. Marmar, J.L. Telly et al., J. Nucl. Mater. 196–198 (1992) 686.
[98] C. Grisolia, Ph. Chendrih, B. Pégourié and A. Grosman, J. Nucl. Mater. 196–198 (1992) 281.
[99] R.V. Budny, D. Coster, D. Stotler et al., J. Nucl. Mater. 196–198 (1992) 462.
[100] P.K. Mioduszewski, J.T. Hogan, L.W. Owen et al., J. Nucl. Mater. 220–222 (1995) 91.
[101] A.V. Markin and A.P. Zakharov, in preparation.
[102] J.W. Davis and A.A. Haasz, these Proceedings, p. 37.